

**Pressure-induced transition in the multiferroic  $\text{CoCr}_2\text{O}_4$  spinel**

I. Efthimiopoulos<sup>1</sup>, Z. T. Y. Liu<sup>2</sup>, S. V. Khare<sup>2</sup>, P. Sarin<sup>3</sup>, T. Lochbiler<sup>1</sup>, V. Tsurkan<sup>4,5</sup>,  
A. Loidl<sup>4</sup>, D. Popov<sup>6</sup>, and Y. Wang<sup>1</sup>

<sup>1</sup>*Department of Physics, Oakland University, Rochester, MI 48309, USA*

<sup>2</sup>*Department of Physics, University of Toledo, Toledo, OH 43606, USA*

<sup>3</sup>*School of Materials Science and Engineering, Oklahoma State University, Tulsa, OK  
74106, USA*

<sup>4</sup>*Experimental Physics 5, Center for Electronic Correlations and Magnetism, Institute  
of Physics, University of Augsburg, D-86159 Augsburg, Germany*

<sup>5</sup>*Institute of Applied Physics, Academy of Sciences of Moldova, MD 2028 Chisinau,  
Republic of Moldova*

<sup>6</sup>*High Pressure Collaborative Access Team, Geophysical Laboratory, Carnegie  
Institution of Washington, Argonne, IL 60439, USA*

**SUPPLEMENTARY INFORMATION**

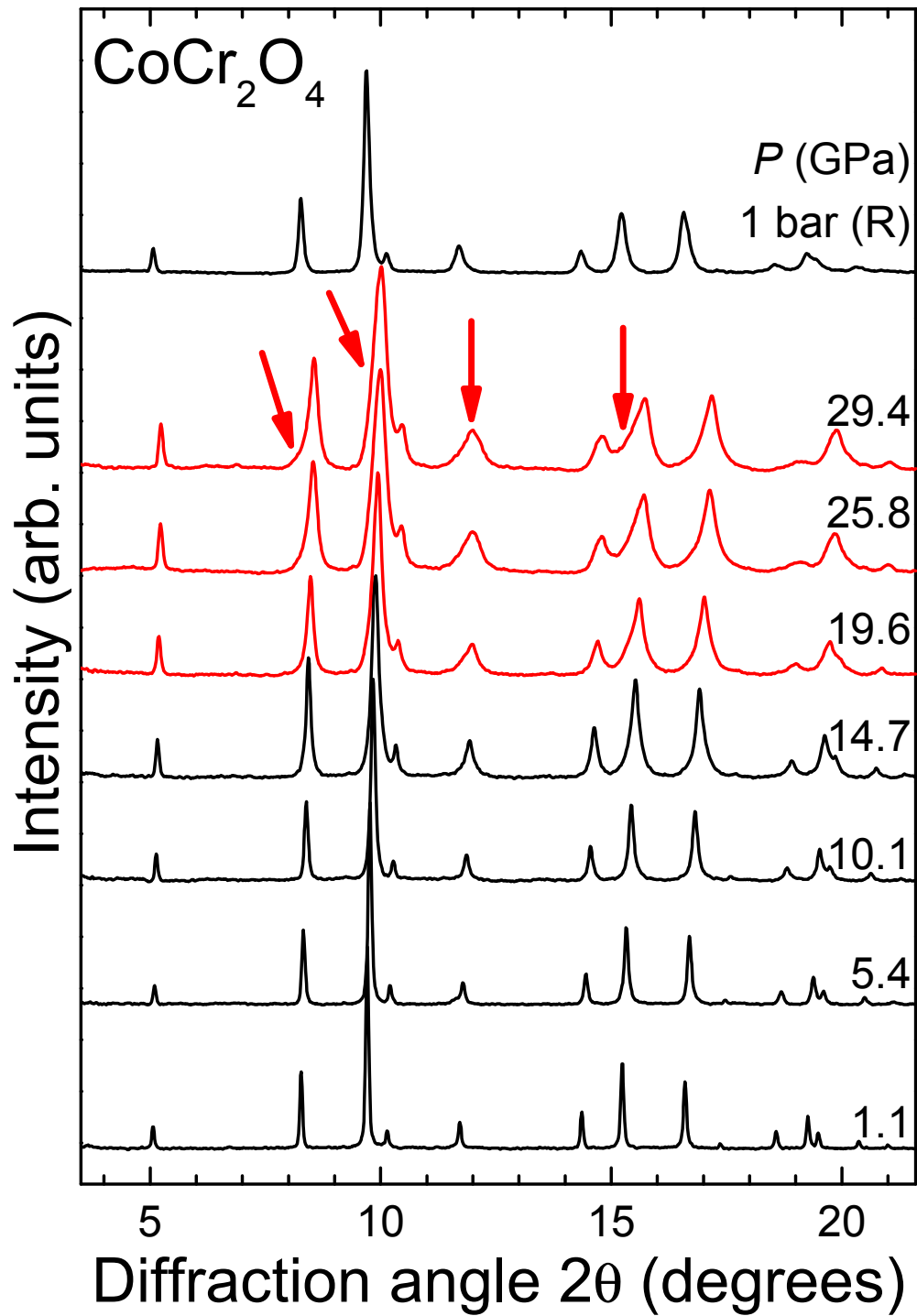


**FIG. S1:** Normalized XRD patterns of  $\text{CoCr}_2\text{O}_4$  at selected pressures ( $T=300$  K,  $\lambda=0.4246$  Å). The black and red patterns correspond to the  $Fd\bar{3}m$  and the tetragonal phases, respectively. Arrows mark the Bragg peak splittings. Background has been subtracted for clarity.

**Table S1:** Experimentally determined structural data (lattice parameters, volume  $V$ , oxygen positional coordinate  $u$ , cation-anion bond lengths, and the Cr-O-Cr bond angle) for the  $Fd-3m$  ( $Z=8$ ) and the  $I4_1/amd$  ( $Z=4$ ) phases of  $\text{CoCr}_2\text{O}_4$ .

$Fd-3m$	$P$ (GPa)	$a$ (Å)	$V$ (Å <sup>3</sup> )	O- $u$	Co-O (Å)	Cr-O (Å)	Cr-O-Cr (degrees)
	0.0001	8.3341(1)	578.86(2)	0.2653(5)	2.026(2)	1.964(1)	97.2(1)
	1.1	8.3203(1)	575.99(2)	0.2655(5)	2.025(2)	1.960(1)	97.3(1)
	2.1	8.3069(1)	573.21(2)	0.2657(5)	2.024(2)	1.955(1)	97.4(1)
	3.1	8.2964(1)	571.04(2)	0.2650(5)	2.012(2)	1.957(1)	97.1(1)
	4.1	8.2845(1)	568.58(2)	0.2646(5)	2.003(2)	1.958(1)	96.8(1)
	5.4	8.2711(1)	565.84(2)	0.2651(5)	2.007(2)	1.951(1)	97.1(1)
	6.6	8.2541(1)	562.35(2)	0.2644(5)	1.993(2)	1.952(1)	96.8(1)
	8.1	8.2354(1)	558.54(2)	0.2637(5)	1.979(2)	1.952(1)	96.4(1)
	10.1	8.2126(1)	553.91(2)	0.2637(5)	1.972(2)	1.948(1)	96.4(1)
	11.8	8.1989(1)	551.14(2)	0.2629(5)	1.958(2)	1.950(1)	96.0(1)
	13.2	8.1829(1)	547.93(2)	0.2630(5)	1.956(2)	1.945(1)	96.1(1)
	14.7	8.1693(1)	545.19(2)	0.2624(5)	1.944(2)	1.946(1)	95.8(1)
	16.3	8.1579(1)	542.93(2)	0.2620(8)	1.936(5)	1.947(4)	95.6(3)
$I4_1/amd$	$P$ (GPa)	$a$ (Å)	$c$ (Å)	$c/a$	$V$ (Å <sup>3</sup> )		
	17.8	5.7649(1)	8.142(1)	0.9987(2)	270.60(4)		
	19.6	5.7591(1)	8.115(1)	0.9963(2)	269.14(4)		
	21.4	5.7572(1)	8.084(1)	0.9928(2)	267.93(4)		
	23.6	5.7509(1)	8.031(1)	0.9875(2)	265.61(4)		
	25.8	5.7451(2)	7.997(1)	0.9842(2)	263.94(5)		
	27.4	5.7408(2)	7.965(3)	0.9811(5)	262.6(1)		
	29.4	5.7312(2)	7.925(3)	0.9778(5)	260.3(1)		

**Table S2:** Theoretically calculated (with DFT) structural parameters (lattice constants and volumes) for the paramagnetic cubic and the ferrimagnetic tetragonal phases of  $\text{CoCr}_2\text{O}_4$  at various pressures. The energy  $E$  of each configuration is also provided.

	$P$ (GPa)	$a$ (Å)	$V$ (Å <sup>3</sup> )	$E$ (eV)		
<b>Paramagnetic cubic</b>	-3.3	8.527	620.00	-419.050		
	0	8.472	608.00	-419.165		
	2.9	8.425	598.00	-419.072		
	10.4	8.320	576.00	-418.159		
	19.3	8.213	554.00	-416.110		
	30	8.103	532.00	-412.705		
	$P$ (GPa)	$a$ (Å)	$c$ (Å)	$c/a^*$	$V$ (Å <sup>3</sup> )	$E$ (eV)
<b>Ferrimagnetic tetragonal</b>	-3.3	6.043	8.489	0.993	310.00	-209.511
	0	6.004	8.433	0.993	304.00	-209.572
	2.9	5.971	8.386	0.993	299.00	-209.525
	10.4	5.909	8.248	0.986	288.00	-209.083
	19.3	5.849	8.098	0.978	277.00	-208.067
	30	5.805	7.894	0.959	266.00	-206.387

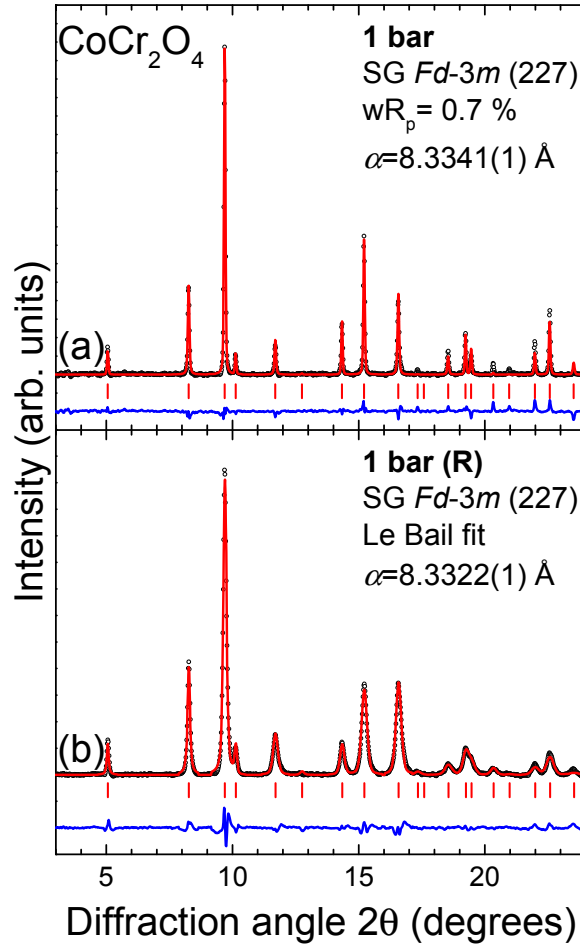


**FIG S2:** Refinements for the  $Fd-3m$  phase of  $\text{CoCr}_2\text{O}_4$  at ambient pressure before [(a), Rietveld] and after [(b), Le Bail fit] after the experimental pressure run. Dots correspond to the measured spectrum, whereas the red and blue solid lines represent the best refinement and the difference between the experimental and refined pattern, respectively. Vertical ticks mark the Bragg peak positions.

**Table S3:** Elastic parameters, i.e. bulk modulus  $B_0$  and its pressure derivative  $B'_0$  for selected oxide spinels. The reported transition pressures  $P_{\text{Tr}}$  and the respective high-pressure (HP) phases are also tabulated.

Spinel	$B_0$ (GPa)	$B'_0$	$P_{\text{Tr}}$ (GPa)	HP phase
$\text{CoCr}_2\text{O}_4$	209( $\pm$ 8)	5( $\pm$ 1)	>16	Tetragonal
	<sup>a</sup> 170( $\pm$ 2)	<sup>a</sup> 4.1( $\pm$ 2)	~10	Tetragonal
$\text{FeCr}_2\text{O}_4$ <sup>1</sup>	209	4	12	$I4_1/amd$
$\text{MgCr}_2\text{O}_4$ <sup>2</sup>	189	7.2	20	$I4_1/amd$
$\text{ZnCr}_2\text{O}_4$ <sup>3</sup>	183	7.9	23	Orthorhombic
$\text{MnCr}_2\text{O}_4$ <sup>4</sup>	252	4.8	20-23	Decomposition
$\text{NiCr}_2\text{O}_4$ <sup>5</sup>	-	-	<sup>a</sup> 16	Decomposition
$\text{CdCr}_2\text{O}_4$ <sup>6</sup>	-	-	10 (+1100 °C)	$\text{CaFe}_2\text{O}_4$ -type
$\text{Co}_3\text{O}_4$ <sup>7,8</sup>	190	6.2	-	-
	249	4	30	$\text{Ag}_3\text{O}_4$ -type

<sup>a</sup>Our *ab initio* calculations.

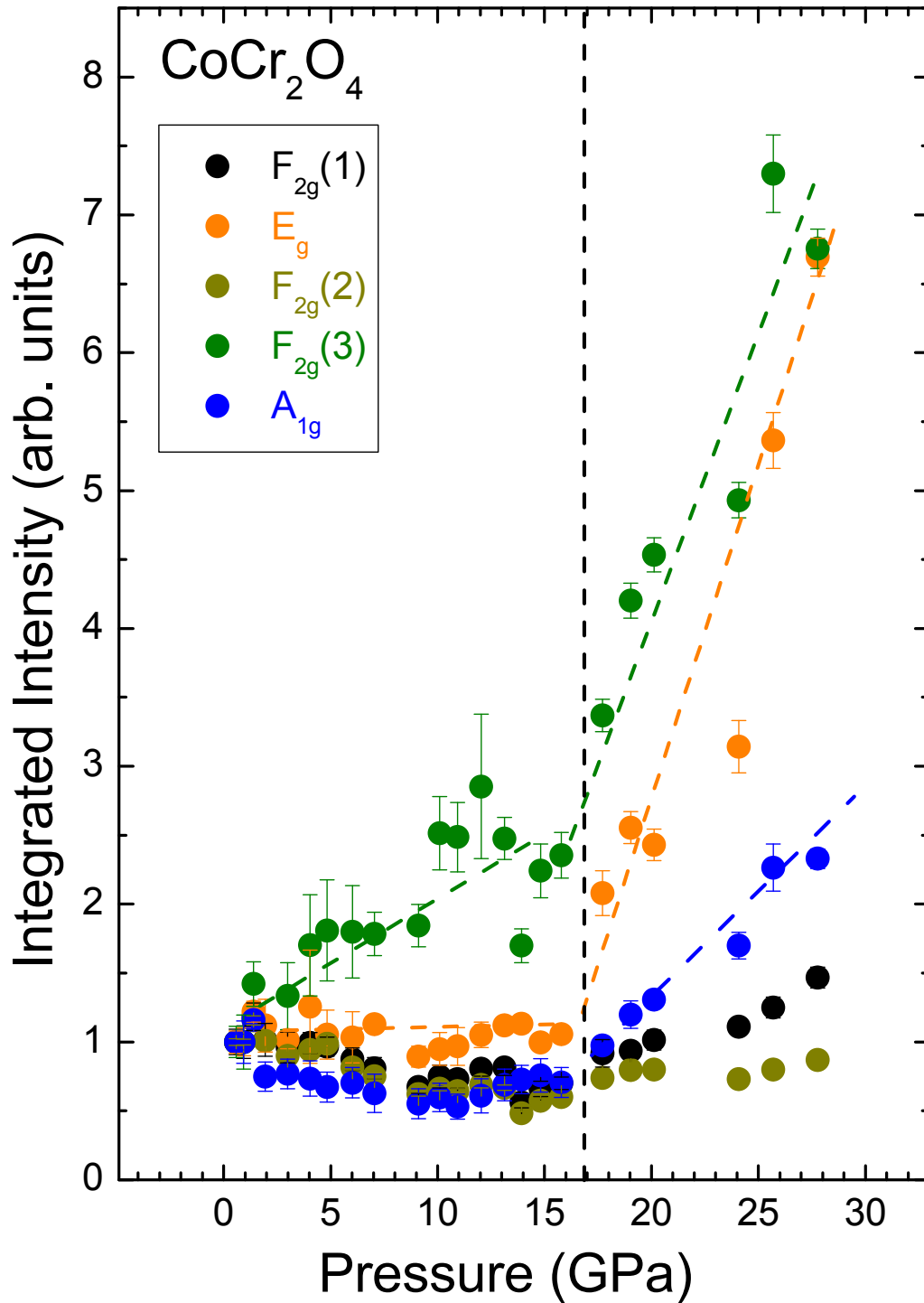


**FIG S3:** Integrated intensities for all of the observed Raman-active modes as a function of pressure. The vertical dashed line marks the onset of the cubic-tetragonal transition.

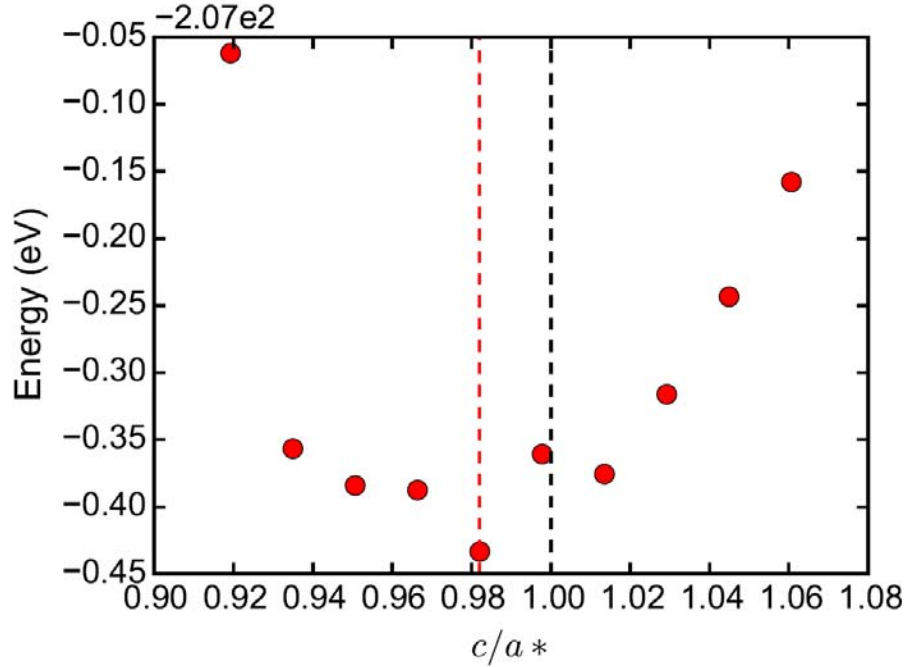
**Table S4:** Construction parameters (lattice vectors and fractional coordinates) for the special quasi-random paramagnetic  $\text{CoCr}_2\text{O}_4$  supercell. The first half of Co and Cr cations are set to spin-up, and the second half spin-down.

Lattice vector ( $\text{\AA}$ )	x	y	z
<b>a</b>	-6.0295128	0	8.5270194
<b>b</b>	6.0295128	0	8.5270194
<b>c</b>	0	6.0295128	-8.5270194

Ion	Fractional coordinates			Ion	Fractional coordinates		
	$u_1$	$u_2$	$u_3$		$u_1$	$u_2$	$u_3$
Co	0.875554	0.875722	0.501083	O	0.330552	0.830808	0.27383
Co	0.125579	0.625537	0.001117	O	0.830985	0.330766	0.274063
Co	0.250916	0.750671	0.502005	O	0.306792	0.306417	0.227742
Co	0.000864	0.000857	0.001472	O	0.806197	0.806594	0.227529
Co	0.375384	0.375415	0.501102	O	0.942313	0.670085	0.498696
Co	0.625897	0.125731	0.001094	O	0.442466	0.169813	0.49861
Co	0.750643	0.250614	0.5012	O	0.919871	0.692478	-0.001364
Co	0.500687	0.500985	0.002139	O	0.420125	0.192364	-0.001275
Cr	0.31349	0.063618	0.501779	O	0.567988	0.56813	0.27411
Cr	0.812463	0.562347	0.500132	O	0.06842	0.068303	0.27397
Cr	0.935828	0.936853	0.248623	O	0.046348	0.546081	0.227744
Cr	0.436639	0.435499	0.248593	O	0.546007	0.046264	0.227705
Cr	0.937123	0.43704	0.248318	O	0.19223	0.419765	-0.001621
Cr	0.437538	0.937725	0.248814	O	0.692693	0.920162	-0.000976
Cr	0.562754	0.812829	0.500899	O	0.169711	0.442213	0.498351
Cr	0.063214	0.313128	0.500993	O	0.670114	0.942655	0.498986
Cr	0.18703	0.187148	0.748344	O	0.9315	0.203597	-0.001691
Cr	0.687753	0.687577	0.748887	O	0.431013	0.703911	-0.000951
Cr	0.813639	0.563484	0.001767	O	0.453916	0.681018	0.499065
Cr	0.312355	0.062511	0.000118	O	0.953577	0.181481	0.498305
Cr	0.68691	0.185819	0.748652	O	0.580789	0.580513	0.773826
Cr	0.185491	0.686694	0.748596	O	0.080733	0.080963	0.774066
Cr	0.063163	0.313226	0.000994	O	0.556627	0.056193	0.727512
Cr	0.562836	0.812727	0.000849	O	0.056434	0.556827	0.727744
O	0.181257	0.954006	0.499165	O	0.318123	0.818002	0.774076
O	0.681344	0.453403	0.498263	O	0.818315	0.3184	0.773981
O	0.703981	0.431256	-0.000851	O	0.796312	0.796058	0.727788
O	0.203427	0.931366	-0.001751	O	0.296091	0.296351	0.727784

**Table S5:** Summations of the Heisenberg model<sup>9</sup> employed for the determination of the magnetic exchange parameters  $J_{AA}$ ,  $J_{AB}$ , and  $J_{BB}$  in  $\text{CoCr}_2\text{O}_4$ .

	Co-Co	Co-Cr	Cr-Cr
Ferromagnetic	8	24	24
Néel-type ferrimagnetic	8	-24	24
Ferrimagnetic in Cr	8	0	-8
Ferrimagnetic in Co	-8	0	24

**FIG S4:** The ferrimagnetic energy surface against the axial ratio  $c/a^*$  at 26 GPa. The energy surface minimum is achieved at  $c/a^*=0.98$ .**Table S6:** Extracted ionic charge transfer from the Bader charge analysis of the paramagnetic cubic and ferrimagnetic tetragonal phases of  $\text{CoCr}_2\text{O}_4$  at various pressures. Notice that the pressure-induced changes of the ionic charge is not much different between the two phases.

	Atomic Species	$q_{trans}$ (C)		
		0 GPa	10 GPa	30 GPa
Paramagnetic cubic	Co	-1.277	-1.271	-1.255
	Cr	-1.777	-1.768	-1.751
	O	1.208	1.202	1.190
Ferrimagnetic tetragonal	Co	-1.284	-1.275	-1.262
	Cr	-1.775	-1.770	-1.754
	O	1.209	1.204	1.192

**References**

- <sup>1</sup> A. Kyono, S. A. Gramsch, T. Yamanaka, D. Ikuta, M. Ahart, B. O. Mysen, H. K. Mao, and R. J. Hemley, *Phys. Chem. Miner.* **39**, 131 (2012).
- <sup>2</sup> W. Yong, S. Botis, S. R. Shieh, W. Shi, and A. C. Withers, *Phys. Earth Planet. Inter.* **196**, 75 (2012).
- <sup>3</sup> D. Levy, V. Diella, A. Pavese, M. Dapiaggi, and A. Sani, *Amer. Miner.* **90**, 1157 (2005).
- <sup>4</sup> M. Catti, F. F. Fava, C. Zicovich, and R. Dovesi, *Phys. Chem. Miner.* **26**, 389 (1999).
- <sup>5</sup> Z. Wang, S. K. Saxena, P. Lazor, and H. S. C. O'Neill, *J. Phys. Chem. Sol.* **64**, 425 (2003).
- <sup>6</sup> A. M. Arevalo-Lopez, A. J. Dos Santos-Garcia, E. Castillo-Martinez, A. Duran, and M. A. Alario-Franco, *Inorg. Chem.* **49**, 2827 (2010).
- <sup>7</sup> L. Bai, M. Pravica, Y. Zhao, C. Park, Y. Meng, S. V. Sinogeikin, and G. Shen, *J. Phys. Cond. Matt.* **24**, 435401 (2012).
- <sup>8</sup> S. Hirai and W. L. Mao, *Appl. Phys. Lett.* **102**, 041912 (2013).
- <sup>9</sup> C. Ederer and M. Komelj, *Phys. Rev. B* **76**, 064409 (2007).